Nanoscale Research Letters

NANO EXPRESS Open Access

In_2S_3 Quantum Dots: Preparation, Properties and Optoelectronic Application

Rujie Li[1,2], Libin Tang[1,2*], Qing Zhao[1*], Thuc Hue Ly[3], Kar Seng Teng[4], Yao Li[5], Yanbo Hu[2], Chang Shu[2] and Shu Ping Lau[6]

Abstract

Low-dimensional semiconductors exhibit remarkable performances in many device applications because of their unique physical, electrical, and optical properties. In this paper, we report a novel and facile method to synthesize In_2S_3 quantum dots (QDs) at atmospheric pressure and room temperature conditions. This involves the reaction of sodium sulfide with indium chloride and using sodium dodecyl sulfate (SDS) as a surfactant to produce In_2S_3 QDs with excellent crystal quality. The properties of the as-prepared In_2S_3 QDs were investigated and photodetectors based on the QDs were also fabricated to study the use of the material in optoelectronic applications. The results show that the detectivity of the device stabilizes at ~ 10^{13} Jones at room temperature under 365 nm ultraviolet light irradiation at reverse bias voltage.

Keywords: In_2S_3 QDs, Preparation, Properties, Optoelectronic application

Background

Graphene-like two-dimensional nanomaterials are of great scientific and technological interests [1, 2]. Currently, there has been growing research interests in developing low-dimensional materials that exhibit unique photoelectric properties [3] and quantum dots (QDs) have gained much attraction [4]. Indium sulfide (In_2S_3) QDs, which belong to the group III–VI semiconductor materials [5], have many unique optoelectrical, thermal, and mechanical properties, which are suitable for numerous potential applications. For example, sulfide nanomaterials have experienced rapid development for use in solar cells [6], photodetectors [7, 8], biological imaging [9], and photocatalytic degradation [10]. There are various ways of preparing sulfide QDs, and they can be divided into two main categories, namely, 'top-down' and 'bottom-up' [11].

However, commonly used bottom-up methods, such as hydrothermal [12], template[13, 14], and microwave methods [15], have many limitations that restrict the widespread application of sulfide QDs [16]. To ensure the successful application of sulfide QDs, it is of paramount importance to develop low-cost, facile preparation method that can produce stable, reliable, and high-quality QDs material [17]. In this article, a novel preparation method that allows synthesis of In_2S_3 QDs at atmospheric temperature conditions has been developed by using indium chloride and sodium sulfide as indium and sulfur source respectively. The physical and photoelectric properties of the as-prepared In_2S_3 QDs were investigated using multiple characterization techniques.

Photoelectric device based on the In_2S_3 QDs were fabricated, and results show the detectivity of the device stabilizes at 10^{13} Jones under 365 nm UV irradiation at room temperature, which demonstrates In_2S_3 QDs have great potential applications in photodetectors. Compared with other growth methods, the reported approach is mild, facile, environmentally friendly, rapid, and cheap. Therefore, it is suitable for low-cost large-scale production of the device that also yields excellent performances. This work demonstrates a low-cost, effective fabrication technique for future application of sulfide QDs in the field of photoelectric detection.

Methods

Materials

Sodium sulfide ($Na_2S{\cdot}9H_2O$) was purchased from Tianjin Wind Ship Chemical Testing Technology Co. Ltd., Tianjin China. Indium chloride ($InCl_3{\cdot}4H_2O$) was obtained from Shanghai Aladdin Biochemical Technology Co.

* Correspondence: scitang@163.com; qzhaoyuping@bit.edu.cn
[1]School of Physics, Beijing Institute of Technology, Beijing 100081, China
Full list of author information is available at the end of the article

Ltd Shanghai, China. Sodium dodecyl sulfate was purchased from Sinopharm Chemical Reagent Co. Ltd., Shanghai, China. Dialysis bag (USA spectrum lab's regenerated cellulose membrane, M_w = 300) was purchased from Shanghai Yibai Economic and Trade Co. Ltd. All of the materials above were purchased commercially and used without further purification.

In_2S_3 QDs Fabrication

In_2S_3 QDs were prepared using the fabrication process as shown in Fig. 1a. Na_2S (0.1 mol/L) and $InCl_3$ (0.1 mol/L) were first dissolved in deionized water. The same volume of Na_2S and SDS(CMC 0.008 mol/L)solutions were mixed using magnetic stirrer for 20 min at 1500 rpm. A mixture of $InCl_3$ and SDS was prepared in the same way. The addition of SDS is to obtain a monodispersed, passivated QDs under a controlled synthesis process. The Na_2S mixture was then added to the $InCl_3$ mixture solution in a beaker to initiate the chemical reaction, which resulted in yellowish products after 10 min. Deionized water was added to the reacted solution and then followed by centrifugation at 3000 rpm for 5 min. The products were washed three times and purified using dialysis bag. The prepared In_2S_3 QDs were collected in the dialysis bag.

Characterization

Transmission electron microscope (TEM) images were obtained with a JEM-2100 high-resolution trans-mission microscope operating at 200 kV. The surface morphology and phase image of photovoltaic devices were determined by scanning electron microscope (SEM, FEI Quanta 200) and AFM (atomic force microscope, SPA-400), respectively. XRD analysis was investigated using a Rigaku D/Max-RA X-ray diffractometer with Cu Ka radiation. Raman spectrum was recorded at ambient temperature on a Renishaw in via Raman microscope with an argon-ion laser at an excitation wavelength of 514.5 nm. Optical properties were characterized by

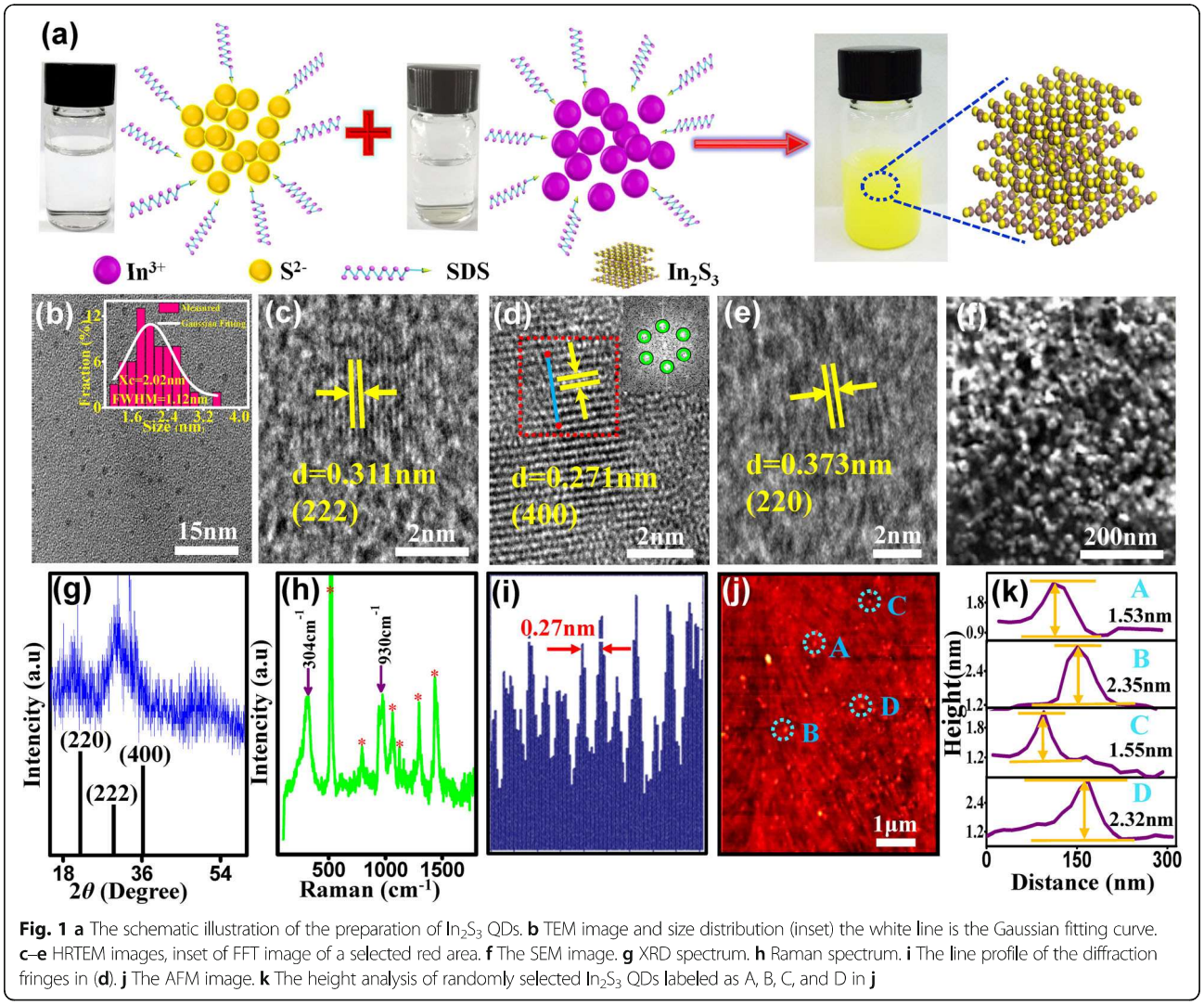

Fig. 1 **a** The schematic illustration of the preparation of In_2S_3 QDs. **b** TEM image and size distribution (inset) the white line is the Gaussian fitting curve. **c–e** HRTEM images, inset of FFT image of a selected red area. **f** The SEM image. **g** XRD spectrum. **h** Raman spectrum. **i** The line profile of the diffraction fringes in (**d**). **j** The AFM image. **k** The height analysis of randomly selected In_2S_3 QDs labeled as A, B, C, and D in **j**

UV-vis, UV-vis-NIR (UV-3600), and fluorescence (Hitachi F-7000) spectrometers. Functional groups on the surface of the In_2S_3 QDs were verified by XPS (X-ray photoelectron spectroscopy) (PHI Versa Probe II) using 72 W, mono Al Ka radiation. *J-V* and *C-V* were measured using Keithley 2400 source meter and semiconductor device analyzer (Keysight B1500A), respectively.

Results and Discussion

Structure and Morphology Studies

TEM images of the In_2S_3 QDs are shown in Fig. 1b–e. It can be seen that In_2S_3 QDs are evenly distributed and exhibit spheroid morphology. Its particle size distribution follows the Gaussian distribution with size ranging from 1 to 3 nm and FWHM of 1.12 nm. The particle has an average size of 2.02 nm. Figure 1c–e are HRTEM images of the In_2S_3 QDs showing its lattice fringes for d = 0.271 nm, 0.311 nm, and 0.373 nm, corresponding to the cubic crystal system of 400, 222, and 220 lattice planes respectively [18]. Figure 1i shows a longitudinal profile of the lattice fringes shown in Fig. 1d. The fast Fourier transform (FFT) pattern of the selected region (red dotted square) is shown in Fig. 1d insert, which reveals six bright spots from the 400 plane diffraction, indicating the crystalline structure of the hexagonal system. The scanning electron microscopy (SEM) image of the as-prepared In_2S_3 QDs is shown in Fig. 1f. As shown, the In_2S_3 QDs agglomerated to form a relatively compact structure in order to reduce its surface energy. X-ray diffraction (XRD) planes at 400, 222, and 220 of the In_2S_3 QDs are shown in Fig. 1g and the calculated particle size using the Sheer formula is in good agreement with the measured size from the 400 plane of HRTEM image. Figure 1h shows Raman spectrum of the In_2S_3 QDs with typical peaks at 304 cm^{-1} and 930 cm^{-1} [19]. Atomic force microscopy (AFM) was performed on four randomly selected In_2S_3 QDs, marked as A, B, C, and D as shown in Fig. 1j, with measured heights of 1.53 nm, 2.35 nm, 1.35 nm, and 2.32 nm (shown in Fig. 1k), respectively. The average height of 1.94 nm from the AFM measurement is very close to that obtained from the TEM.

The estimated band gap of In_2S_3 QDs is 3.50 eV, which is larger than its bulk value of 2.3 eV, due to the quantum effect. The band gap was calculated using the Brus equation:

$$E_{np} \approx E_{g(0)} + \frac{\overline{h}^2 \pi^2}{2R^2}\left(\frac{1}{m_e{}^*} + \frac{1}{m_h{}^*}\right) - \frac{1.8e^2}{4\pi\varepsilon R} \quad (1)$$

where E_{np} is the bandgap of the QDs, E_g is the band gap of bulk In_2S_3 (2.3 eV), $\overline{h}$ =h/2π is the reduced Planck constant, e is the electron charge, $m_e{}^*$ is the effective mass of electron, $m_h{}^*$ is the effective mass of hole, $m_e{}^* = m_h{}^*(0.25 \times 10^{-28}\mathrm{g})$, R is the radius of the particle and ε is the dielectric constant (ε = 11).

Figure 2a shows ultraviolet-visible (UV-vis) absorption spectra of the In_2S_3 QDs. There are two characteristic peaks of absorption located at 225 nm and 283 nm [20]. Since In_2S_3 is a direct bandgap material, its optical band gap can be expressed by the following equation:

$$\alpha h\nu = A(h\nu - Eg)^{1/2} \quad (2)$$

where α is the absorption coefficient, A is a constant, $h\nu$ is the photo energy, and Eg is the band gap energy.

The band gap energy of the QDs can be estimated from the curve of $(\alpha h\nu)^2$ vs. photo energy ($h\nu$). The estimated E_g of 3.54 eV, as shown in the inset of Fig. 2a, is very close to the calculated value using the Brus equation (E_{np}=3.50 eV). Photoluminescence (PL) and photoluminescence excitation (PLE) [21] studies were performed to investigate the optical properties of the In_2S_3 QDs. It can be seen from Fig. 2b that there is an emission peak at a wavelength between 300 and 450 nm, and the strongest peak intensity is centered at ~ 390 nm under the excitation of E_x = 250 nm. PLE spectra in Fig. 2c show that wavelengths of the characteristic excitation peaks are shorter than the receiving wavelengths (500–540 nm). The broadening of energy gap of In_2S_3 QDs compared to its bulk material may also be demonstrated by PL and PLE results. The fluorescence of the In_2S_3 QDs under visible light and 365 nm UV light are shown in Fig. 2c insert. This demonstrates that the In_2S_3 QDs possess good UV fluorescence properties. X-ray photoelectron spectroscopy (XPS) was also performed to study the chemical bonds of the In_2S_3 QDs. Figure 2d shows the XPS full scan spectrum, which consists of S2p at 162.5 eV, $In3d_{5/2}$ at 444.5 eV, and $In3d_{3/2}$ at 452.5 eV. Besides, there are residual Cl, Na, O, and C from the surfactant and reactant. Core level peaks of S2p and In3d are shown in Fig. 2e, f respectively. The deconvoluted peaks reveal the bonding states of S2p (In-S, C-S), $In3d_{5/2}$. (In-S, In-O), and $In3d_{3/2}$ (In-S, In-O).

As the In_2S_3 QDs demonstrated excellent ultraviolet absorption properties, UV photodetector based on the In_2S_3 QDs was fabricated and investigated. The preparation process is illustrated in Fig. 3a.

The specification of the Au interdigitated electrodes is similar to that reported by Tang. et al. [22], consisting of electrodes with a thickness of 400 nm, a length of 120 μm, and width and spacing of 10 μm. Figure 3b shows an optical image of empty electrodes. Fig. 3c, d shows the optical microscopic images showing the spacing of the electrodes filled with the In_2S_3 QDs, which acted as a photosensitive layer. The measured current density against voltage (*J-V*) and log (*J-V*) curves of the device in dark condition, irradiated by 0.16 mW cm^{-2} and 0.47 mW cm^{-2} power density of 365 nm UV light

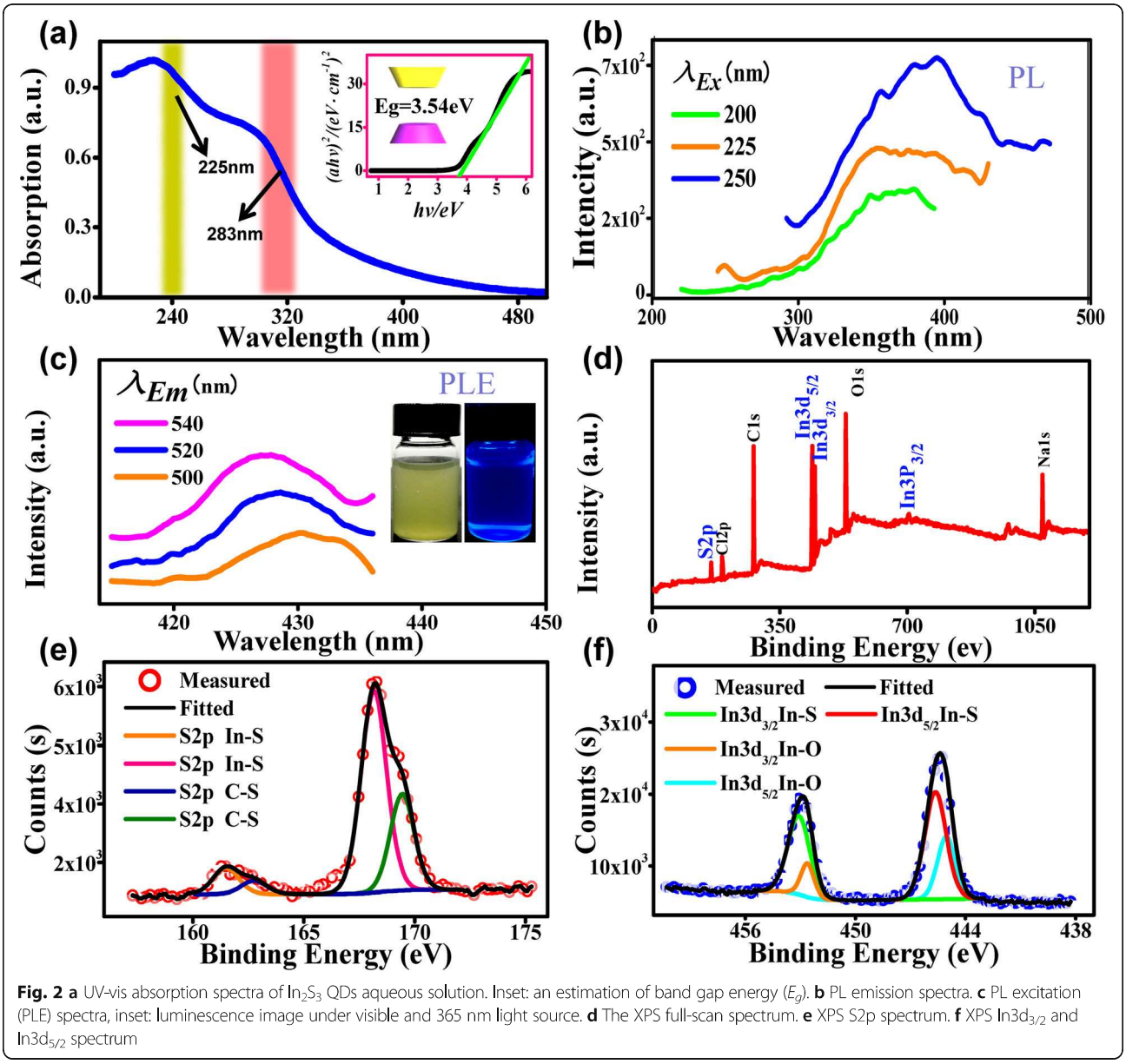

Fig. 2 **a** UV-vis absorption spectra of In_2S_3 QDs aqueous solution. Inset: an estimation of band gap energy (E_g). **b** PL emission spectra. **c** PL excitation (PLE) spectra, inset: luminescence image under visible and 365 nm light source. **d** The XPS full-scan spectrum. **e** XPS S2p spectrum. **f** XPS $In3d_{3/2}$ and $In3d_{5/2}$ spectrum

are shown in Fig. 3e, f respectively. An increase in the current density is observed when the irradiated power density increases, hence demonstrating the characteristics of a rectifier. The responsivity (R) and detectivity (D^*) of the photodetector are calculated using the following equations:

$$R = J_{ph}/P_{opt} \tag{3}$$

$$D* = \frac{R}{\sqrt{2q/jd}} \tag{4}$$

where J_{ph} is the photocurrent density, P_{opt} is the photo power density, q is the absolute electron charge (1.6×10^{-19} coulombs), and J_d is the dark current density [23]. From Fig. 3g, the maximum value of R is 4.13 A W^{-1}, which is significantly larger than that of graphene and many other two-dimensional nanomaterial devices [24, 25] and is seen to increase with an increase in the reverse bias voltage. As shown in Fig. 3h, the D^* is stabilized at around 10^{13} Jones.

The optical images of empty electrodes and those filled with In_2S_3 QDs are shown in Fig. 4a. The plot of R-T measured from the In_2S_3 QDs-based photodetector at a voltage of 1 V and 2 V is shown in Fig. 4b. It shows that an increase in temperature has led to a decrease in the resistance; however, it does not exhibit a simple linear relationship. In order to understand the electrical properties of the In_2S_3 QDs, the $\ln(\rho)$-$1/T$ of the device was attained and the results are shown in Fig. 4c. By using the two model equations [26]:

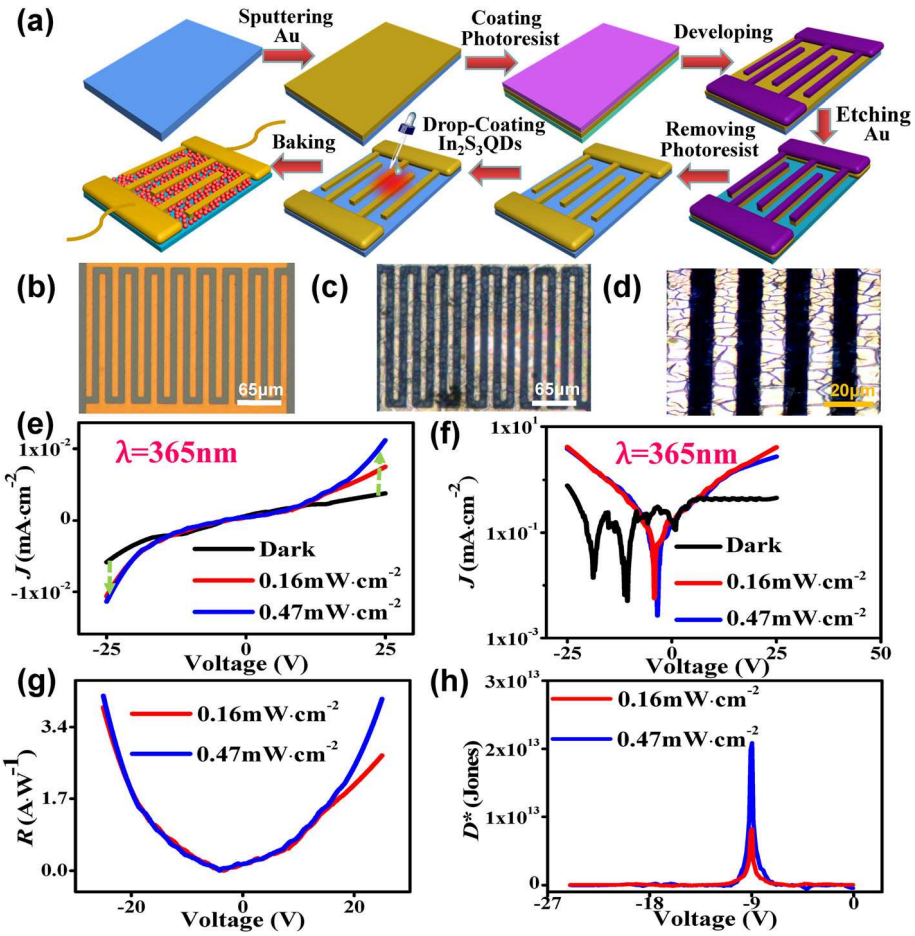

Fig. 3 **a** Schematic diagram illustrating the fabrication process of the In_2S_3 QDs UV photovoltaic detector. **b** Electrode without QD. **c–d** Optical microscopic images of the In_2S_3 QDs photodetector at different magnifications. **e–h** Performance of the In_2S_3 QDs detector. **e** *J-V* curves. **f** Log *(J)-V* curves. **g** *R* (responsivity)-*V* curves. **h** *D**

$$\rho = R\frac{(N-1)wd}{l} \tag{5}$$

$$\mathrm{In}\,(\rho) = \mathrm{In}\,(A) + E_a/\,(k_b \cdot T) \tag{6}$$

where N is the number of interdigitated electrodes, w is the overlapping length, l is the spacing, and d is the thickness of the film [27]. Using a simple linear regression, the calculated thermal activation energy (E_a) is 0.011 eV and the finger-leading factors (A) is 4.16 × 10^8 Ω°cm. The thermal activation energy of In_2S_3 QDs could be reduced as long as the obtained energy is sufficient for the carriers to participate in conduction, which can result in lower resistivity and higher conductivity.

Generally, *C-V* measurements can provide many important information on the nature of the semiconductor interface and charge transport. Fig. 4d shows that capacitance decreases with increasing frequency and the decrease in capacitance is significant at low frequencies. This is due to the interface states, which respond to the alternating current signal, and the presence of the interface states would suppress the AC signal at high frequency, hence resulting in a weakened trend or a constant capacitance. Figure 4e shows the *C-V* curves of the In_2S_3 QDs-based photodetector at room temperature with a frequency of 40 MHz. The *C-V* relationship under a bias can be expressed as [28]

$$C^{-2} = \frac{2(V_{bi}-V)}{q\varepsilon_0\varepsilon_r NS^2} \tag{7}$$

where V_{bi} is the built-in potential at zero bias, ε_0 is the permittivity of vacuum, ε_r is the relative permittivity of a material, N is the carrier concentration in the depletion layer and S is the photosensitive area (3.3 mm^2). The x-intercept is V_{bi} = 0.6 V, and the carrier concentration N can be calculated from the slope of the linear section of $1/C^2$ vs. V plot [29]: $N = \frac{-2}{q\varepsilon_0\varepsilon_r A^2}\left[\frac{\partial(C^{-2})}{\partial V}\right]^{-1}$, and the calculated N=4.3 × 10^{19} cm^{-3}. The depletion width (W_d) is between the electrode and the In_2S_3 QDs layer, expressed as W_d

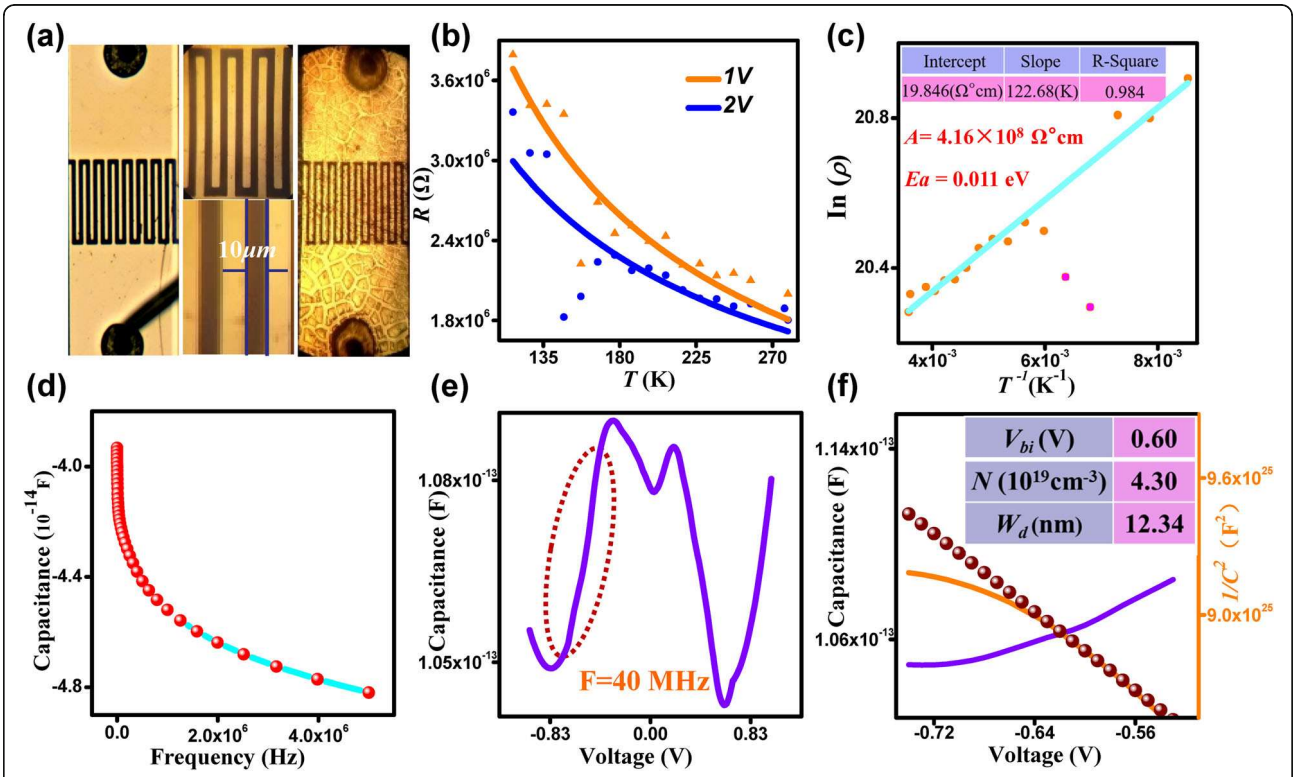

Fig. 4 **a** Photodetector with In_2S_3 QDs as an active layer. **b** Plot of R-T at 1 V and 2 V. **c** Plot of *ln (ρ)-1/T*-based devices at 1 V. **d** *C-F* curves measured at room temperature. **e** The *C-V* curves (40 MHz)-based photodetector in the dark condition. **f** Variation of the capacitance with applied voltages and plots of $1/C^2$ vs. *V* of the device

$= \left[\frac{2\varepsilon_0\varepsilon_r(V_{bi}-V)}{qN}\right]^{1/2}$, the calculated W_d = 12.34 nm. These physical parameters are shown in Fig. 4f. It is evident that the V_{bi} and W_d are the same as similar QDs devices (such as the graphene quantum dots) [30], but the N is larger by an order of magnitude at zero bias. This explains the excellent performances of the device as compared to other QDs device [31].

Conclusions

A novel and facile preparation method to produce high crystal quality In_2S_3 QDs was developed. The structural, optical, electrical, and photovoltaic properties of the In_2S_3 QDs have been studied. In the dark field condition, the activation energy (E_a), finger-leading factor (A), built-in potential (V_{bi}), and depletion layer width (W_d) of the UV photodetector based on In_2S_3 QDs were obtained. In_2S_3 QDs were used as the sole photoactive material in the fabricated photodetector that exhibits the highest detectivity (D^*) of 2×10^{13} Jones at room temperature under 365 nm UV light illumination without preamplifier. This method is ideal in developing high performance, large array of In_2S_3 QDs-based UV photoelectric detector at very low cost.

Abbreviations

AFM: Atomic force microscope; CMC: Critical micelle concentration; FFT: Fast Fourier transform; FWHM: Full width at half maximum; HRTEM: High-resolution transmission electron microscope; PL: Photoluminescence; PLE: Photoluminescence excitation; QDs: Quantum dots; SDS: Sodium dodecyl sulfate; SEM: Scanning electron microscope; TEM: Transmission electron microscope; XPS: X-ray photoelectron spectroscopy; XRD: X-ray diffractometer

Acknowledgements

This work was supported by National Natural Science Foundation of China (No. 61106098), Equipment Pre-research Fund under the Equipment Development Department (EDD) of China's Central Military Commission (CMC) (No.1422030209), and the Innovation Team Program of NORINCO Group (No.2017CX024).

Availability of Data and Materials

The conclusions made in this manuscript are based on the data (main text and figures) presented and shown in this paper.

Authors' Contributions

RL carried out the experiments and drafted the manuscript. LT designed the experiments. LT and QZ supervised the experiments. THL, KST, and SPL participated in the discussion and analyzed the experimental results. LT, THL, KST, and SPL helped to draft and revise the manuscript. YL, YH, and CS helped to characterize the samples. All authors read and approved the final manuscript.

Competing Interests

The authors declare that they have no competing interests.

Publisher's Note

Author details
[1]School of Physics, Beijing Institute of Technology, Beijing 100081, China. [2]Kunming Institute of Physics, Kunming 650223, Yunnan Province, China. [3]Department of Chemistry, City University of Hong Kong, Kowloon Tong, Hong Kong. [4]College of Engineering, Swansea University, Bay Campus, Fabian Way, Swansea SA1 8EN, UK. [5]School of Materials Science and Engineering, Yunnan University, Kunming 650091, China. [6]Department of Applied Physics, The Hong Kong Polytechnic University, Hung Hom, Kowloon, Hong Kong.

Received: 1 March 2019 Accepted: 26 April 2019
Published online: 14 May 2019

References

1. Atatüre M, Englund D, Vamivakas N, Lee S-Y, Wrachtrup J (2018) Material platforms for spin-based photonic quantum technologies. Nat Rev Mater. 3(5):38–51
2. Callicó GM (2017) Graphene: Image sensors go broadband. Nature Photon 11(6):332–333
3. Cheng J-Y, Fisher BL, Guisinger NP, Lilley CM (2017) Atomically manufactured nickel–silicon quantum dots displaying robust resonant tunneling and negative differential resistance. npj Quantum Mater 2(1)
4. Li X, Zhao Y-B, Fan F, Levina L, Liu M, Quintero-Bermudez R, Gong X, Quan LN et al (2018) Bright colloidal quantum dot light-emitting diodes enabled by efficient chlorination. Nature Photon 12(3):159–164. https://doi.org/10.1038/s41566-018-0105-8
5. Souissi R, Bouguila N, Labidi A (2018) Ethanol sensing properties of sprayed β-In_2S_3 thin films. Sensors and Actuat B: Chem 261:522–530. https://doi.org/10.1016/j.snb.2018.01.175
6. Ho C-H (2012) The study of below and above band-edge imperfection states in In_2S_3 solar energy materials. Physica. B 407:3052ve ban
7. Butanovs E, Butikova J, Zolotarjovs A, Polyakov B (2018) Towards metal chalcogenide nano wire-based colour-sensitive photodetectors. Optical Mater. 75:501–507
8. Ho C-H, Lin M-H, Wang Y-P, Huang Y-S (2016) Synthesis of In_2S_3 and Ga_2S_3 crystals for oxygen sensing and UV photodetection. Sensors and Actuators A 245:119ng dio
9. Kui Y, Ng P, Ouyang J, Zaman MB, Abulrob A et al (2019) Low-temperature approach to highly emissive copper indium sulfide colloidal nanocrystals and their bioimaging applications. ACS Applied Materials & Interfaces 5:2870–2880
10. Zhang X, Zhang N, Gan C, Liu Y, Chen L, Fang CZY (2019) Synthesis of In_2S_3/UiO-66 hybrid with enhanced photocatalytic activity towards methyl orange and tetracycline hydrochloride degradation under visible-light irradiation. Materials Science in Semiconductor Processing 91:212–221
11. Bera A, Mandal D, Goswami PN, Rath AK, Prasad BLV (2018) Generic and scalable method for the preparation of monodispersed metal sulfide nanocrystals with tunable optical properties. Langmuir 34(20):5788–5797
12. Buchmaier C, Rath T, Pirolt F, Knall A-C, Kaschnitz P, Glatter O, Wewerka K, Hofer F, Kunert B, Krenn K, Trimmel G (2016) Room temperature synthesis of $CuInS_2$ nanocrystals. RSC Adv 6(108):106120–106129
13. Ho C-H (2010) Growth and characterization of near-band-edge transitions in β-In_2S_3 single crystals. J Crystal Growth 312(19):2718–2723
14. Konstantatos G, Sargent EH (2011) Colloidal quantum dot photodetectors. Infrared Phys & Technol 54(3):278–282
15. Li Z, Yang T, Zhao X, Zhao Q, Yu H, Zhang M (2017) Doping-concentration-induced ferromagnetism and antiferromagnetism in In_2S_3:Dy^{3+} quantum dots. J Phys. Chem C 121(17):9648–9654
16. Li J, Ma Y, Ye Z, Zhou M, Wang H, Ma C, Wang D, Huo P, Yan Y (2017) Fast electron transfer and enhanced visible light photocatalytic activity using multi-dimensional components of carbon quantum dots@3D daisy-like In $_2$ S $_3$ /single-wall carbon nanotubes. Appl Catal B: Environ 204:224–238
17. Ghosh S, Saha M, Ashok VD, Chatterjee A, De SK (2016) Excitation dependent multicolor emission and photoconductivity of Mn, Cu doped In_2S_3 monodisperse quantum dots. Nanotech 27(15):155708
18. Wang X, Hwang JY, Myung ST, Hassoun J, Sun YK (2017) Graphene Decorated by Indium Sulfide Nanoparticles as High-Performance Anode for Sodium-Ion Batteries. ACS Appl Mater Interfaces 9(28):23723–23730
19. Karthikeyan S, Hill AE, Pilkington RD (2017) Low temperature pulsed direct current magnetron sputtering technique for single phase β-In_2S_3 buffer layers for solar cell applications. Appl Surf Sci 418:199–206
20. Li Y, Wang Q, Gao Y, Liu B, Gao C, Ma Y (2017) Investigation on morphological properties of In_2S_3 by high pressure x-ray diffraction. Mater Research Express 4(8):085902
21. Lhuillier E, Keuleyan S, Guyot-Sionnest P (2013) Colloidal quantum dots for mid-IR applications. Infrared Phys & Technol 59:133–136
22. Feng J, Zhu H, Yang X (2013) A controllable growth-doping approach to synthesize bright white-light-emitting Cd:In_2S_3 nanocrystals. Nanoscale 5(14):6318–6322
23. Tang L, Ji R, Li X, Bai G, Liu CP, Hao J, Lin J (2014) Deep Ultraviolet to Near-Infrared Emission and Photoresponse in Layered N-Doped Graphene Quantum Dots. ACS Nano 8(6):6312–6320
24. Huang W, Gan L, Yang H, Zhou N, Wang R, Wu W, Li H, Ma Y, Zeng H, Zhai T (2017) Controlled Synthesis of Ultrathin 2D β-In_2S_3 with Broadband Photoresponse by Chemical Vapor Deposition. Adv Funct Mater 27(36). https://doi.org/10.1002/adfm.201702448
25. Lutfi Abdelhady A, Ramasamy K, Malik MA, O'Brien P (2013) Very narrow In_2S_3 nanorods and nanowires fro m a single source precursor. Mater Lett 99:138–141
26. Cakmakyapan S, Lu PK, Navabi A, Jarrahi M (2018) Gold-patched graphene nano-stripes for high-responsivity and ultrafast photodetection from the visible to infrared regime. Light: Sci & Appl 7(1). https://doi.org/10.1038/s41377-018-0020-2
27. Sumi R, Warrier AR, Vijayan C (2014) Visible-light driven photocatalytic activity of β-indium sulfide (In_2S_3) quantum dots embedded in Nafion matrix. J Phys D: Appl Phys 47(10)
28. Jianghong Zhao, Libin Tang, JinZhon Xiang, Rongbin Ji, Yanbo Hu, Jun Yuan,Jun Zhao,Yuhua Cai (2015) Fabrication and properties of a high-performance chorine doped graphene quantum dot based photovoltaic detector. RSC Advances 5:29222
29. Martyniuk P, Rogalski A (2008) Quantum-dot infrared photodetectors: Status and outlook. Prog Quant Electron 32(3-4):89–120
30. Pejova B, Bineva I (2013) Sonochemically synthesized 3D assemblies of close-packed In2S3 quantum dots: structure, size dependent optical and electrical properties. J Phys Chem C 117(14):7303–7314
31. Zhao J, Tang L, Xiang J, Ji R, Hu Y, Yuan J, Zhao J, Tai Y, Cai Y (2015) Fabrication and properties of a high-performance chlorine doped graphene quantum dot based photovoltaic detector. RSC Adv 5(37):29222–22922